frontiers | Frontiers in Earth Science

TYPE Original Research
PUBLISHED 17 July 2024
DOI 10.3389/feart.2024.1416594

OPEN ACCESS

EDITED BY
Jianguo Zhang,
China University of Geosciences, China

REVIEWED BY
Mabrouk Sami,
United Arab Emirates University, United Arab Emirates
Qinghai Xu,
Yangtze University, China

*CORRESPONDENCE
Xiaohong Liu,
liuxiaohong_swpu@163.com

RECEIVED 12 April 2024
ACCEPTED 18 June 2024
PUBLISHED 17 July 2024

CITATION
Lin T, Wang W, Ma Q, Kang J, Yang R and Liu X (2024), Formation mechanism and implication of analcime in the sandstone reservoirs of the Permian Jingjingzigou formation in the Jinan sag, southern Junggar basin, NW China. *Front. Earth Sci.* 12:1416594. doi: 10.3389/feart.2024.1416594

Formation mechanism and implication of analcime in the sandstone reservoirs of the Permian Jingjingzigou formation in the Jinan sag, southern Junggar basin, NW China

Tong Lin[1], Weiwei Wang[2,3], Qiang Ma[4], Jilun Kang[4], Runze Yang[1] and Xiaohong Liu[2]*

[1]Research Institute of Petroleum Exploration and Development, PetroChina, Beijing, China, [2]School of Geoscience and Technology, Southwest Petroleum University, Chengdu, China, [3]Sinopec Henan Oil-field Company, Nanyang, China, [4]Research Institute of Exploration and Development, Tuha Oilfield Company, PetroChina, Hami, China

Analcime plays a significant role in sandstone reservoirs as an authigenic diagenetic mineral in the Junggar Basin (northwestern China). However, the origin and controls on the reservoirs have received remarkably little attention. This study investigates the formation mechanism of analcime in the Middle Permian strata in the Jinan sag (southern Junggar Basin) through petrography and geochemistry. The results show that analcime is formed through early alkaline hydrolysis of volcanic materials under specific temperature and pressure conditions. The reservoir rocks primarily consist of various lithic sandstones, including volcanic debris such as basalt, andesite, and tuff. Analcime is characterized as rich in aluminium and poor in sodium, classified as low-silica analcime with a low Si-Al ratio (1.98–2.38). Furthermore, various other diagenetic minerals, such as glauconite, chlorite, albite, and calcite have been identified. The primary reservoir space chiefly consists of intragranular dissolved pores of analcime, while secondary pores are formed by intragranular pores of feldspar and lithic, along with some remaining intergranular pores. Cementation of analcime during early diagenesis changes primary pore structures and reduces reservoir properties. The low-silica analcime dissolves due to acidic pore fluids associated with three stages of oil and gas charging, transforming into albite and creating numerous secondary pores, thereby enhancing reservoir quality.

KEYWORDS

Northwestern China, Junggar basin, Permian, sandstone reservoir, analcime, secondary pore, diagenetic evolution

1 Introduction

Zeolite Minerals significantly impact on oil and gas reservoirs (Iijima, 2001). During the diagenetic evolution process, diagenesis involving the precipitation, dissolution, and transformation of authigenic zeolite minerals, directly affects the pore evolution

of sandstone reservoirs, therefore influencing reservoir performance (Sun et al., 2014; Zhu et al., 2020). Analcime as a common type of zeolite minerals, pervasively occurs in oil and gas bearing basins such as central Australia (English, 2001), northwestern Argentina (Campo et al., 2007), Canada (Gall and Hyde, 2010), Turkey (Varol, 2020), western and eastern China (Lin et al., 2017; Fang et al., 2020).

Despite the causes and formation environments of analcime have been studied, but the results are controversial. Renaut (1993) summarized four formation mechanisms of authigenic analcime in sandstone: 1) alteration of volcanic glass and zeolite precursors; 2) formation from a gel; 3) direct precipitation of interstitial pore fluid or lake water; and 4) reactions of saline, alkali pore water with detrital silicates (e.g., clay and plagioclase). Sheppard and Hay (2001) and Langella et al. (2001) systematically discussed the occurrence, formation conditions and genetic characteristics of authigenic analcime, suggest water chemistry, temperature and pressure composed influenced the formation. Guo et al. (2022) proposed that the lower the concentration ratio of hydrogen ions to alkali metal ions in the formation water, the more conducive it is to the formation of zeolite minerals. In addition, the pH value of the pore water may control the types of zeolites formed: neutral to moderate pH values are conducive to the formation of zeolite with a high Si/Al ratio, while aluminium-rich zeolite (e.g., analcime) is more likely to be formed at a high pH value (Jin and Boles, 1993; Neuhoff, 2002). The larger the silica-to-alumina ratio of zeolite minerals, the stronger the acid resistance; otherwise, the acid resistance is low and zeolite minerals are easily dissolved by it.

Partly scholars suggested that the precipitation and filling of zeolite minerals have a destructive effect on the original pore structure in the early stage, leading to a reduction in primary pores and a decrease in reservoir performance (Taylor and Surdam, 1981; Noh and Boles, 1993; Utada, 2001). However, the presence of analcime cement can also enhance the strength of the reservoir structure, improve its resistance to compaction, and inhibit compaction-induced reduction in porosity. Additionally, the analcime cement can indirectly provide a material basis for later acidic fluids (e.g., organic acids) to cause dissolution (Schmidt and McDonald, 1979; Dutton and Loucks, 2010; Fu et al., 2010; Yuan et al., 2015). Weibel et al. (2019) indicated that thermogenic degradation of early zeolite cementation can create deep-buried sandstone reservoirs with abnormally high porosity and permeability levels. In the middle diagenetic stage, the analcime cement formed in the early stage can undergo widespread dissolution, resulting in the formation of secondary pores, enhanced porosity and permeability, and ultimately improved reservoir quality (Zhu et al., 2011; Meng et al., 2013; Sun et al., 2014).

Terrigenous clastic rock reservoirs are the primary oil and gas reservoirs in western China (Jia, et al., 2016; Zheng, et al., 2019). For instance, in the Junggar Basin (northwest China), clastic reservoirs hold almost all proven oil reserves and over half of the natural gas reserves. High-quality secondary reservoirs of clastic rocks, characterized by intergranular dissolution pores, are closely linked to the cementation of authigenic zeolite minerals (Zhu et al., 2011; Wang et al., 2022; Gao et al., 2023). Various researchers have investigated the formation mechanism of zeolite-based high-quality secondary reservoirs in China's oil- and gas-bearing basins and discussed the reservoir distribution (Zhang, 1985; Han et al., 2007; Li et al., 2014; Sun et al., 2014; Li et al., 2019; Yuan et al., 2020; Zhu et al., 2020; Li et al., 2022). Zhu et al. (2020) provided a review of the occurrence, composition, and origin of analcime sourced from Permian to Paleogene sedimentary rocks in nonmarine petroleum basins in China. The review indicates that the formation of natural analcime is influenced by factors such as the of parent material composition, temperature during crystallization, chemical properties of fluid, and thermodynamic characteristics of the geological environment. Particularly, the Junggar Basin has developed high-quality secondary reservoirs related to analcime cementation facies (Zhu et al., 2020). Diagenetic analcime, found in forms like pyroclastic sandstone and conglomerate intergranular cement, is the most common type of analcime. Analcime is speculated to form during the burial stage of diagenesis through the alteration of minerals such as volcanic glass, clay, or zeolite precursors. It often occurs together with other authigenic zeolites, carbonates, clay minerals and albite, and plays a significant role in controlling the reservoirs quality (Tang et al., 1997a; Tang et al., 1997b; Zhu et al., 2011).

It was identified through exploration in the new Permian Jingjingzigou Formation in the Jinan Sag (NW China, Junggar Basin). The Jinan Sag, along with high-yield oil and gas, presents a total exploration potential of 100 million tons (Liang et al., 2021). Preliminary research shows that analcime is the most common zeolite mineral in the Permian Jingjingzigou Formation, with paragenetic minerals including chlorite, carbonate, and albite. However, the zeolite-related diagenesis and its impacts on reservoir development have not been thoroughly studied. This study utilizes various methods such as cast thin sections, scanning electron microscopy (SEM), whole rock-clay mineral X-ray diffraction, electron probe, and fluid inclusion analyses to examine the development characteristics and related diagenesis of analcime in the Permian Jingjingzigou Formation reservoirs in the Jinan Sag. The primary objectives of this study are to determine the origins of analcime and to assess the impact on reservoirs.

2 Geological setting

The Junggar Basin is one of the main oil and gas-bearing basins in Northwest China. It is an extremely superimposed basin formed by the superposition and composite of several prototype basins with different properties, and it has a complicated evolutionary history. Multiple sets of primary rock-reservoir-caprock assemblages have developed in the basin with very rich hydrocarbon resources. Since the Permian period, the Junggar Block has been in the development and reformation stages of intraplate basins, and it has experienced a complex evolutionary history featuring the early differentiation of uplifts and depressions, the formation of unified basins, and the superposition of later foreland basins (Zhang and Zhang, 2006).

Located in the southern margin of the Junggar Basin, the Jinan Sag is a recently discovered Permian fault depression with an NW-SE direction half-graben structure, similar to the Jimsar Sag. The Jinan Sag is a small sedimentary sag recently discovered in the footwall of the Fukang fault zone's eastern segment in the Junggar Basin's south margin. The Jinan Sag adjoins the Guxi uplift to the east and the Santai uplift to the west; it is bounded to the north by the Jinan uplift, it faces the Jimsar Sag and it is adjacent to the hanging wall of the eastern segment of the Fukang fault zone to the south. The

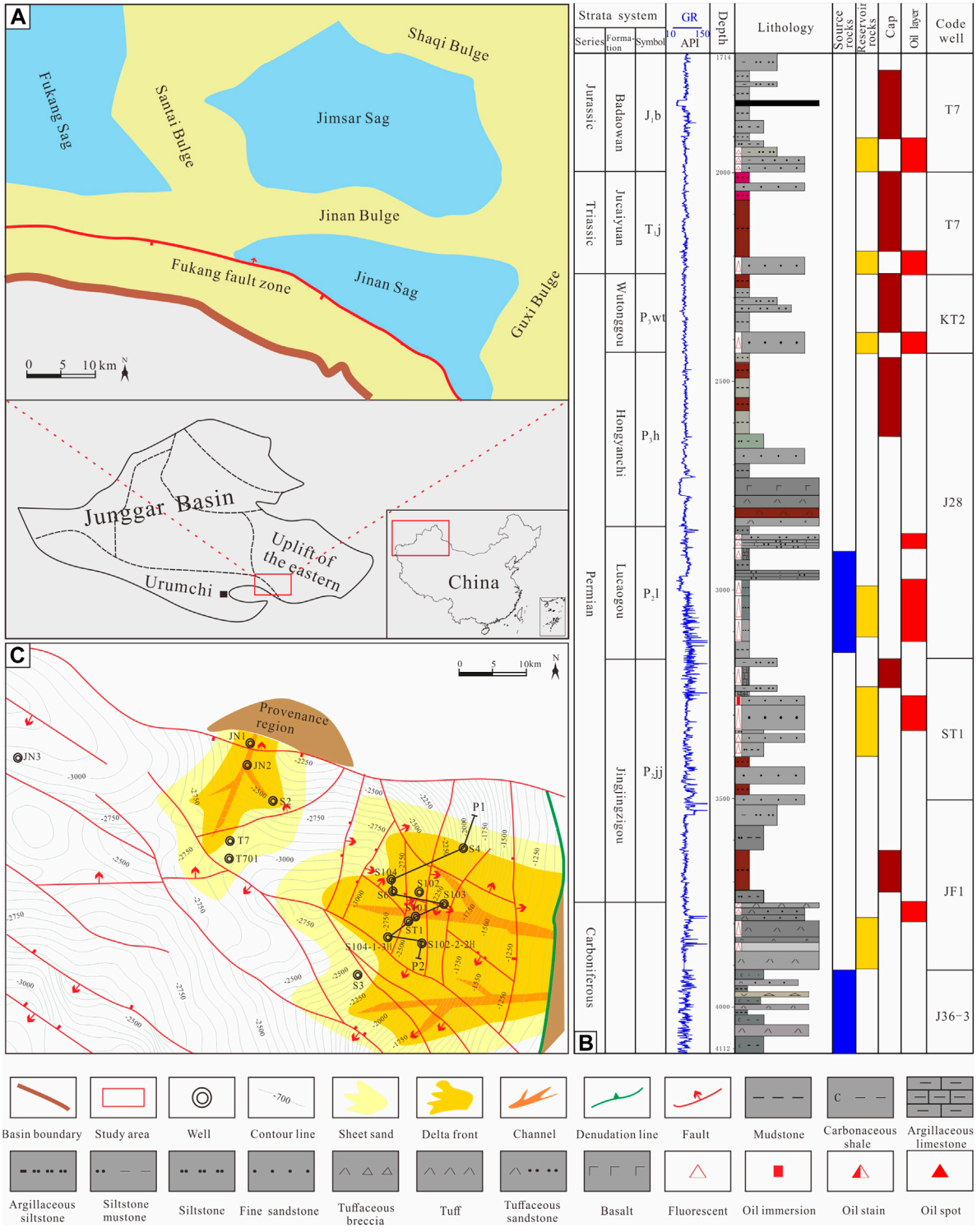

FIGURE 1
Structure location **(A)**, stratigraphic column **(B)** and sandstone distribution **(C)** of the Permian Jingjingzigou Formation in the Jinan Sag.

Jinan Sag has experienced the superposition and transformation of multiphase tectonic movements, such as the Hercynian, Indosinian, Yanshanian, and Himalaya; faults have developed in the sag with obvious thickness in the east and thinness in the west (Wu et al., 2013; Liang et al., 2021) (Figure 1A).

The middle and upper Permian wells in the Jinan Sag have developed from the bottom upwards, including the Jingjingzigou Formation (P_2jj), the Lucaogou Formation (P_2l), the Hongyanchi Formation (P_2h), and the Wutonggou Formation (P_3wt) (Figure 1B). The Jingjingzigou Formation is the primary clastic rock reservoir

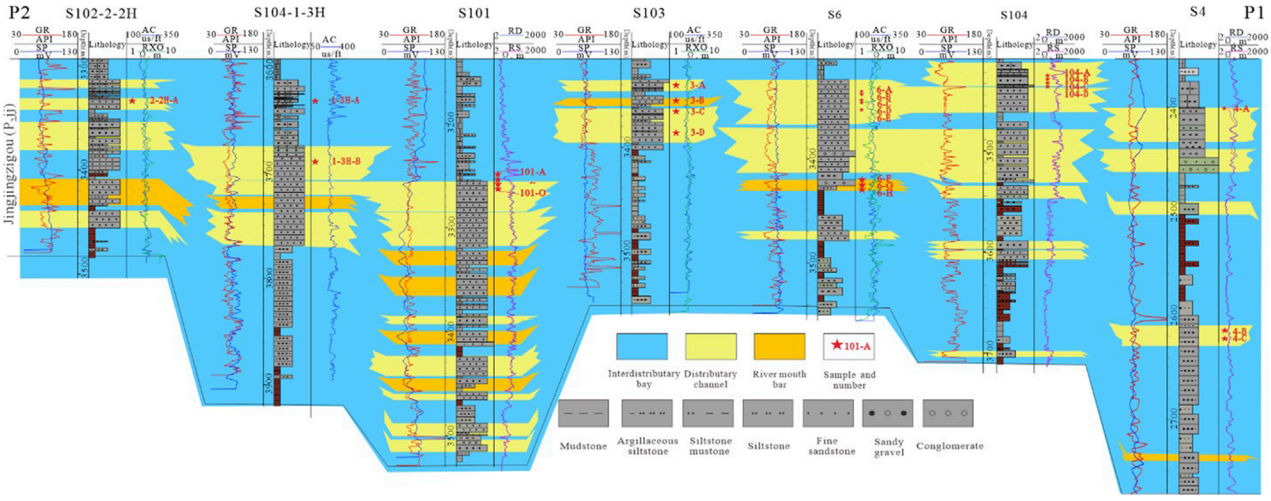

FIGURE 2
Profile of sedimentary facies of the Permian Jingjingzigou Formation in the Jinan Sag. (Line P1-P2 is shown in Figure 1B).

in the Jinan Sag, while the Lucaogou Formation serves as a shale reservoir and is in a conformity contact with the overlying Lucaogou Formation. The upper member features thick sandstone and a high sandstone-stratum ratio, whereas the lower member consists mainly of interbedded red mudstone and grey fine-siltstone. The Lucaogou Formation is characterized by a predominance of continuous thick grey-black mud shale, serving as high-quality hydrocarbon source rocks and effective regional caprocks. The geological setting of Jinan Sag is influenced by the provenance area of the Guxi uplift, resulting in the development of an east-west delta plain facies–delta front facies–shallow lacustrine sedimentary system (Figure 1C). In general, the Jingjingzigou Formation of the Permian is a widely distributed far-source new bed-generating and old bed-storing accumulation lithological reservoir, featuring a favorable source rock–reservoir–caprock configuration (Li et al., 2023). The sandstones are main deposited in delta environment, and the distributary channel and river mouth bar are favorable sedimentary facies for the development of sand bodies (Figure 2).

3 Samples and methods

Based on core observations and descriptions, thin sections (30 samples) were cast from seven drilled wells (S101, S102-2-2H, S103, S104, S104-1-3H, S4 and S6) for observation and quantitative statistics. For mored detailed descript the petrography and highlight difference of reservoirs which bearing analcime, we preferred choose samples of high porosity sandstones, and consider the siltstones with high porosity and relative dense sandstones.The experimental instrument used was an Olympus BX53M reflected polarizing microscope. The thin sections were cast with blue epoxy resin to identify rock pores, stained with alizarin red + potassium ferricyanide mixture to differentiate authigenic carbonate minerals qualitatively, and the thin section porosity, pore size, and pore distribution were measured (12 samples) using Tiger 3000P polarizing image processing software. The fluid-inclusion measurement (10 samples) of Goldstein and Reynolds (1994) was employed for experimentation at Southwest Petroleum University, which involved the use of a Linkam THMSG600 system. Scanning electron microscopy observations (5 samples) were conducted on pore development in the reservoirs and the paragenetic assemblage of authigenic minerals, while electron probe analysis (5 samples) was completed with 60 points on authigenic minerals, such as clays, zeolites, and carbonates in reservoir pores. Both scanning electron microscopy and electron probe analyses were carried out at the State Key Laboratory of Oil and Gas Reservoir Geology and Exploitation, Southwest Petroleum University. For scanning electron microscopy, the specimens were made into block samples and sprayed with gold on their surfaces, while for electron probe analysis, the specimens were ground into polished thin sections and sprayed with carbon on their surfaces. The experimental instruments included an FEI Quanta 650 FEG field emission scanning electron microscope (configured with Qemscan software for minerals recognition) and JXA-8230 electron probe analyzer. The electron probe created spectra after testing the contents of nine common elements in carbonate minerals. The accuracy of spectrum analysis exceeded 1% (major element content >5%) and 5% (minor element content 1%–5%); it could automatically identify elements above 0.1 wt%, and the detection limit was 0.01 wt%. The State Key Laboratory of Oil and Gas Reservoir Geology and Development Engineering conducted an analysis of 20 samples using X-ray diffraction on both whole-rock and clay minerals. The analysis was performed with an X'Pert PRO analyzer, where the detection criterion was set to a maximum current of 60 mA and a pressure of 60 kV. The temperature range was maintained at 23–30°C, while the humidity level was kept above 70% to ensure accurate results.

4 Results

4.1 Reservoir characteristics

Observations and statistics of the cast thin sections show that the reservoir rocks in the study area are mainly lithic sandstone,

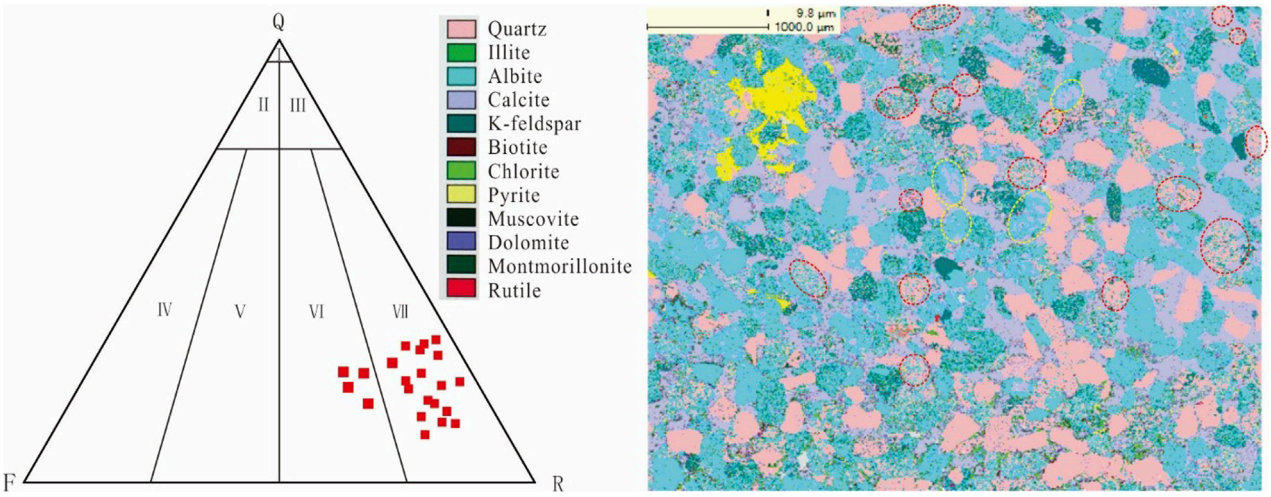

FIGURE 3
Ternary diagram of rock classification (Left) and distribution of the mineral components (Right) of the Jingjingzigou Formation. I- quartz sandstone; II- feldspar-quartz sandstone; III- lithic quartz sandstone; IV- feldspar sandstone; V- lithic feldspar sandstone; VI- feldspar lithic sandstone; and VII- lithic sandstone cement. Q-quartz, F-feldspar, R-rock fragments. Detrital compositions are mainly composed of quartz, feldspar and debris. A large amount of calcite cement was found at Well S104, 3440.16 m.

with a small amount of feldspar lithic sandstone in some wells (Figure 3 left). The general content of debris is between 55% and 70%, and the types include extrusive rock debris, such as basalt, andesite, and tuff, a small amount of sedimentary rock debris, such as siltstone and mudstone, and metamorphic rocks, such as quartzite and phyllite. The plastic debris is significantly transformed into pseudo matrix. The quartz is mainly monocrystalline quartz, with a small amount of polycrystalline quartz, and the secondary enlargement of quartz does not occur. The plagioclase is mainly intermediate acid plagioclase with developed polysynthetic twin, and the potassium feldspar is mainly orthoclase and striated feldspar, with the surface generally kaolinized. The results of whole-rock X-ray diffraction analysis show that the quartz content in the rocks is between 23.8% and 33.3% (Table 1), which is consistent with the detrital quartz content obtained from microscopic thin section statistics, indicating that quartz mainly occurs in the form of detrital quartz and is rarely seen in debris. The potassium feldspar content in the rocks is between 2.7% and 4.8%, and the plagioclase content reaches 46.3%–64.5%. The Qemscan images and statistical results show that, in addition to the single-crystal quartz in the rocks, a small amount of fine-grained quartz is observed in the chert and siltstone debris (red circle in Figure 3 right). The plagioclase is mainly composed of albite feldspar with a relatively small content of potassium feldspar; the phenomena of calcite replacing the potassium feldspar in the striped feldspar and retaining albite stripes can be found (yellow circle in Figure 3 right). The particle size analysis shows that the mean value of the debris particle size is between 0.1 mm and 0.6 mm; the median particle size is 0.18–0.27 mm, and the average particle size is 0.16–0.24 mm. The sorting index (σ_1) is 1.61–1.89, indicating that the sample is fine-medium sandstone with poor sorting. The roundness of particle size is mainly subangular, which is generally supported by grains, with the main line contact between grains and local point contact (Figures 3, 4).

4.2 Mineral characteristics of analcime

Based on the observations of cast thin sections, scanning electron microscopy, electron probe, and X-ray diffraction analyses, authigenic mineral analcime is commonly present in the reservoirs of the Jingjingzigou Formation. In particular, analcime is known to fill intergranular pores with varying degrees of dissolution (Figures 4A–F; Figures 5A–G). Within these pores, analcime may either dissolve, creating a harbor-like structure, while coexisting with albite, or exhibit a complete/hollow equiaxed granular form, occasionally wrapped by calcite minerals. The particle size of analcime ranges from 20 μm to 60 μm, with a maximum size of 100 μm, and a content exceeding 15% (Figures 4A–F; Figures 4A–G). Quantitative electron probe analysis indicates that analcime has an average SiO_2 content of 58.16% (above the standard value of 54.58%), Al_2O_3 concentrations ranging mainly between 23.46% and 24.30% (slightly above the standard value of 23.16%), and an average Na_2O content of 11.12% (considerably below the standard of 13.5%) (Table 2). The calculated average Si/Al ratio of analcime in the study area is 2.14, with values ranging from 1.98 to 2.38, indicating it is a low-silica analcime (Table 2).

4.3 Minerals paragenetic with analcime

In the study area, the reservoirs within the Jingjingzigou Formation commonly contain paragenetic minerals such as analcime, along with clay minerals, albite, calcite, and other minerals. Dissolution processes vary across different areas, leading to transformations where analcime can convert to albite or be replaced by calcite or other minerals (Figures 4A–F; Figures 5A–G). Therefore, analyzing these paragenetic minerals can elucidate the mineral paragenetic sequence, providing a basis for investigating the genetic mechanism of analcime.

TABLE 1 Mineral composition of the Permian Jingjingzigou Formation in the Jinan Sag (%).

Sample ID	Depth (m)	Wells	Clay mineral (%)	Felsic minerals (%)			Carbonate minerals (%)	Zeolite minerals (%)	Clay mineral (%)			Smectite (%)
			Total	Q	K-F	P	Cal	Anl	Sme	Ill	C/S	C/S
101-B	3254.73	S101	4	31	4	45	5	9	4	3	93	38
101-D	3255.52	S101	4	35	4	45	4	7	4	2	94	34
101-F	3256.44	S101	2	40	4	37	9	7	3	4	93	41
101-G	3257.66	S101	3	32	4	43	10	8	4	2	94	38
101-H	3258.30	S101	5	38	0	45	4	8	7	2	91	38
101-I	3259.67	S101	4	41	4	40	2	9	3	5	92	49
101-K	3261.06	S101	4	34	4	48	3	7	3	2	95	45
101-M	3262.17	S101	2	33	4	40	13	8	4	4	92	41
101-O	3263.12	S101	4	35	4	39	11	7	2	5	93	38

Abbreviation: Q, quartz; K-f, K-feldspar; P, plagioclase; Cal, Calcite; Anl, Analcime; Sme, Smectite; Ill, Illite; C/S, Mixed layer Chlorite/Smectite.

Firstly, authigenic albite has been developed in the study area, mainly appearing as lath-shaped crystals filling intergranular pores under the microscope, showing a negative low protrusion. The highest interference colour is off-white in the first order (Figures 4A,B,G–I). When observed under the scanning electron microscope, albite is primarily seen in plate-shaped forms occupying intergranular or analcime dissolution pores, displaying a good euhedral degree (Figure 5). Electron probe analysis reveals that albite mainly consists of Ab, ranging from 98.98% to 99.61%, with only trace amounts of potassium feldspar (Or) and anorthite (An) components present.

In addition, chlorite is mainly distributed along the margins of the pores (encapsulated debris grains) in the form of a film-like pore liner cement with varying degrees of development (Figures 4A,F). In the intergranular dissolution pores of some well sections, the chlorite film is obviously separated from the clastic grains and exists as pore fillings (Figures 4G, 5B,F), indicating that it undergoes a certain degree of corrosion after formation. X-ray diffraction results of clay minerals show that the total amount of clay minerals is between 5.2% and 6.4%, with chlorite accounting for 55.4%–60%, and the mixed chlorite/smectite layer (C/S%) accounting for 37.5%–42.6%. The ratio of smectite (S%) in the chlorite/smectite mixed layer (C/S %) is 40% (Table 1).

Besides, calcite is relatively abundant in some intervals. Based on the staining of the cast thin sections, calcite can be categorized into three types: calcite, ferroan calcite, and ferrocalcite. Calcite appears mainly as microcrystalline grains filling the analcime dissolution pores or as continuous crystals. The mixed solution turns red when intergranular pores are filled; ferroan calcite and ferrocalcite mainly fill the intergranular pores and partial corrosion pores in the shape of continuous crystals, with the mixed solutions stained purple and blue, respectively (Figures 4D–H). It is imperative to acknowledge that the time of calcite formation and the subsequent dissolution during the later phases of diagenesis play a vital role in their influence on the reservoir. According to the quantitative analysis results of the electron probe, it is evident that calcite can be classified into three distinct stages. During these stages, there is a noticeable and consistent increase in the MnO content. In contrast, the FeO content is lowest during the first stage, while the SrO content is highest in the third stage (Figures 6A,B). It can be inferred that calcite undergoes partial dissolution during the first two stages, indicating an earlier formation time. Furthermore, ferrocalcite, the most recent cement, exhibits less dissolution (Figures 5D–H).

Based on the occurrence and paragenetic mineral characteristics of analcime minerals, four paragenetic evolution sequences related to analcime diagenetic minerals can be summarized as follows: ① chlorite → analcime → ferroan calcite (minor quantity). This sequence is mainly observed in Well S101 and Well S4. ② chlorite → analcime → calcite → ferroan calcite → ferrocalcite. This sequence is predominantly found in Wells S101, S104, and S104-1–3H. ③ chlorite → analcime → albite → ferroan calcite (minor quantity). This sequence is mainly identified in Well S101. ④ chlorite → albite → (sphene) → calcite (minor quantity). This sequence is primarily noted in Wells S6 and S102-2-2H. In the above sequences, when the chlorite film has a low development level and the clastic grains are not completely wrapped, small amounts of secondary authigenic quartz enlargement and authigenic feldspar can form on the edges of quartz and feldspar grains (Figures 4G,Q).

4.4 Fluid inclusions

Fluid inclusion analysis is mostly used as an effective tool to investigate the formation condition of analcimes. 10

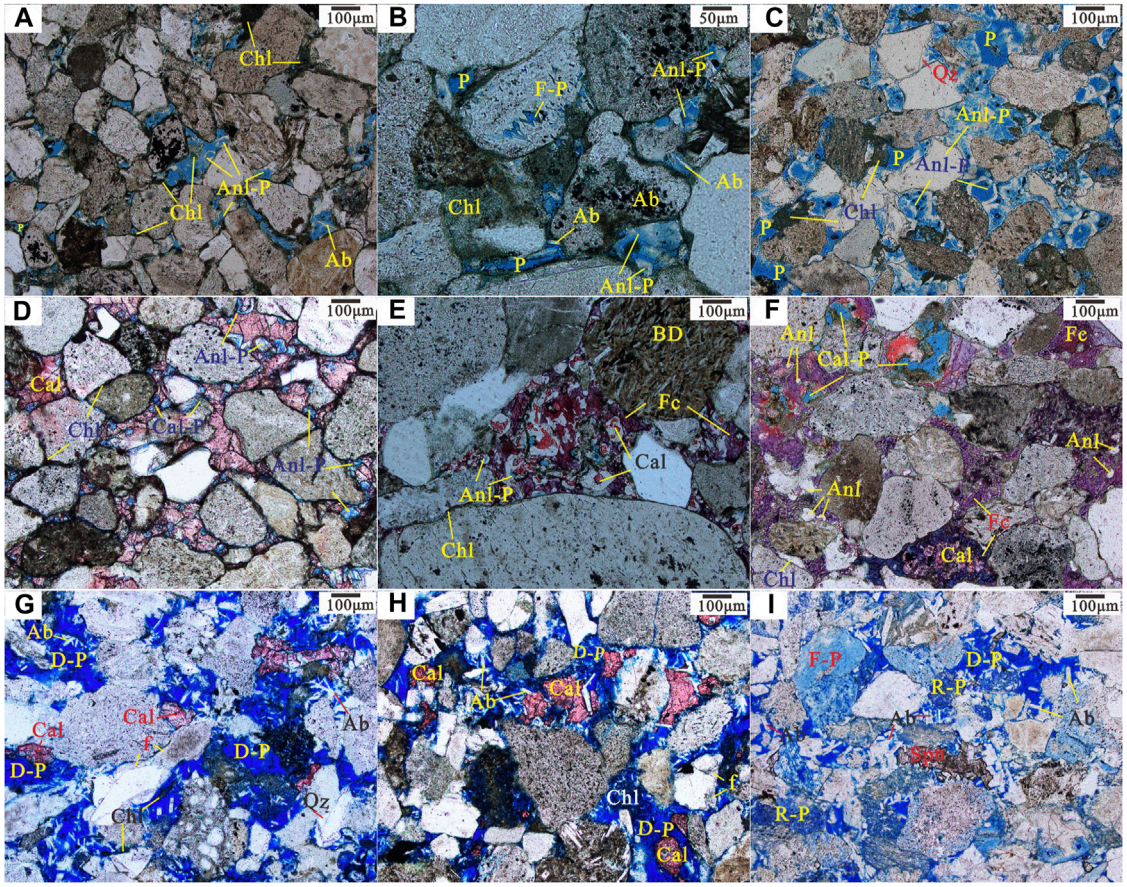

FIGURE 4
Microscopic images of petrography and reservoir space. **(A)** Lithic sandstone, chlorite encapsulated clastic grains, partially filled intergranular pores, developed intergranular analcime dissolution pores, occasional authigenic albite feldspar in the dissolution pores, and additional observed residual intergranular pores (Well S101, 3255.07 m, single polarized light). **(B)** Lithic sandstone, chlorite encapsulated clastic grains, partially filled intergranular pores, developed intergranular analcime dissolution pores, authigenic albite feldspar in the dissolution pores, and a small amount of residual intergranular pores (Well S101, 3262.52 m, single polarized light). **(C)** Feldspar lithic sandstone, weak chlorite film development, locally enriched chlorite, a large amount of filled intergranular analcime, developed analcime dissolution pores, and a small amount of residual intergranular pores (Well S4, 2399.59 m, single polarized light). **(D)** Detritus sandstone, chlorite film-calcite sequentially filled intergranular pores, complete chlorite film, developed analcime dissolution pores, calcite-filled intergranular pores in continuous crystals, and local weak corrosion (Well S104-1-3H, 3478.20 m, single polarized light). **(E)** Detritus sandstone, typical basalt debris, chlorite film developed on grain edge, intergranular pores filled with analcime, dissolution pores partially filled by calcite (red) and residual intergranular pores filled with ferrocalcite (purple-red) (Well S101, 3043.58 m, single polarized light). **(F)** Lithic sandstone, sequentially filled intergranular pores with chlorite-calcite (red)-ferroan calcite (purple-red)-ferrocalcite (blue-purple), intact analcime crystal form, and partially corroded calcite forming secondary dissolution pores (Well S104, 3440.16 m, single polarized light). **(G)** Lithic sandstone, strong dissolution, chlorite film detached from the clastic grains and locally enriched, intergranular pores filled with authigenic albite and partially calcite, calcite-encapsulated albite feldspar, and local phenomenon of authigenic feldspar (Well S102-2-2H, 3334.30 m, single polarized light). **(H)** Lithic sandstone, intensive corrosion, locally enriched chlorite, intergranular pores filled with authigenic albite and partially calcite, calcite-encapsulated albite, and local authigenic feldspar (Well S6, 3343.15 m, single polarized light). **(I)** Feldspar lithic sandstone, strong corrosion, various developed corrosion pores, undeveloped chlorite, and intergranular pores filled with authigenic albite and partially wrapped in authigenic sphene (Well S6, 3421.50 m, single polarized light). Cal: calcite; Fc: ferrocalcite; Chl: chlorite; Ab: albite; (F): feldspar; Spn: sphene; Anl: analcime; Anl-P: analcime dissolution pores; Cal-P: calcite dissolution pores; FP: feldspar dissolution pores; RP: debris dissolution pores; D-P: intergranular dissolution pores; and P: residual intergranular pores; BD: basalt debris; Qz: quartz.

fluid-inclusion analyses of the analcimes in Well S101 are measured (Table 3; Figures 7A,B). The fluid inclusions from analcimes have homogenization temperatures ranging from 78.5°C to 85.1°C, with a comparatively low average of 81.9°C (Figure 7C). The ice melting temperatures ranging from −1.3 to −0.8°C, with an average of −1.1°C. The salinities of the primary fluid inclusions with an average of approximately 1.82 wt% (Figure 7D).

5 Discussion

5.1 Origin of analcime and paragenetic minerals

The types of fragments in the Jingjingzigou sandstones in the Jinan Sag varied. The fragment components were mainly intermediate–basic volcanic rocks. Moreover, there were

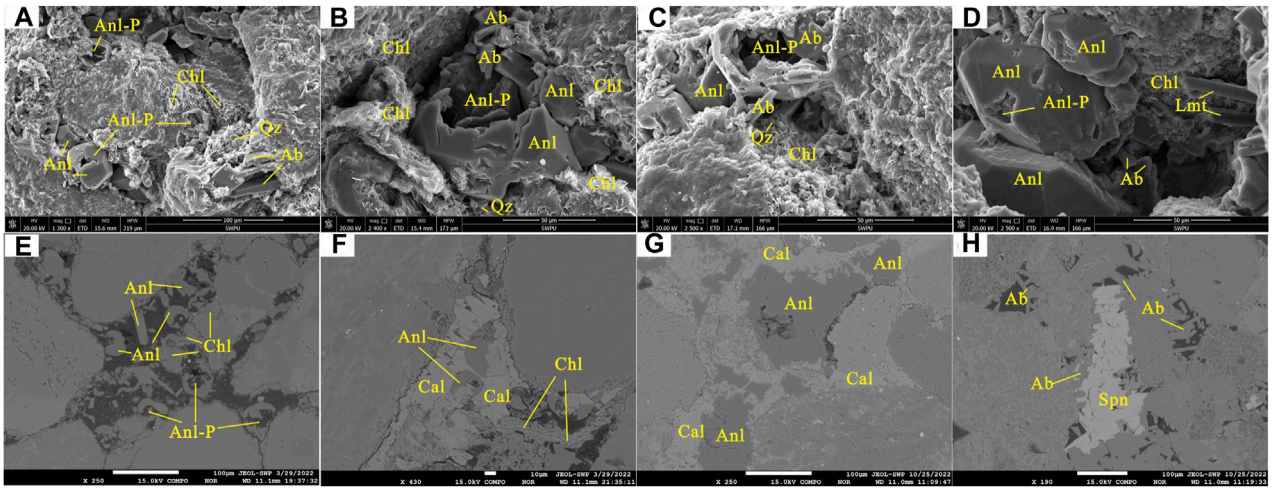

FIGURE 5
Characteristics of analcime and paragenetic minerals under Scanning electron microscopy (SEM) **(A–D)** and Backscattered electron (BSE) **(E–H)**. **(A)** Chlorite encapsulates clastic grains and fills the pores in a plate-like morphology. Equiaxed granular analcime occupies the intergranular pores and undergoes a certain degree of dissolution. Plate-like albite is observed filling the intergranular pores. Authigenic quartz particles are situated between chlorite crystals (Well S101, 3255.07 m, SEM). **(B)** The chlorite film is partially detached from the clastic particles. Analcime is locally dissolved. Dissolution pores are filled with plate-like albite. Authigenic quartz particles are sporadically detected between the chlorite crystals (Well S101, 3255.07 m, SEM). **(C)** Chlorite encases clastic grains. Analcime is evidently dissolved and appears hollow. Plate-like albite is present in the dissolved pores. Authigenic quartz particles are intermittently found between the chlorite crystals (Well S101, 3262.52 m, SEM). **(D)** The chlorite crystal structure is poorly developed. The intergranular analcime is subject to localized dissolution. The intergranular dissolution pores are filled with albite, as exhibited in laumontite (Well S101, 3262.52 m, SEM). **(E)** Significant corrosion of chlorite film and analcime is observed. Intergranular pores are evident (Well S101, 3043.58 m, backscattered electron (BSE)). **(F)** The chlorite is corroded and detached from the detrital grains. The analcime dissolves into a harbor shape and is enveloped by calcite (Well S101, 3261.40 m, BSE). **(G)** Analcime corrosion is not readily apparent. The intergranular pores are filled with encapsulated calcite (Well S6, 3421.50 m, BSE). **(H)** The intergranular dissolution pores are filled with authigenic albite and partially enclosed by authigenic sphene (Well S104-1-3H, 3692.00 m, BSE). Cal: calcite; Chl: chlorite; Ab: albite; Spn: sphene; Anl: analcime; Lmt: laumontite; Qz-quartz; and Anl-p: dissolution pores of analcime.

sedimentary tuff layers with smectite contents greater than 90% in some well intervals (Figure 8A). Between these layers, a large amount of analcime mineral was replaced by calcite, and euhedral dolomite grew coaxially along the bioclasts (Figure 8B). The analcime content in the sandstone above this layer could reach 15%, suggesting that the formation of zeolite minerals was closely related to the genesis of volcanic materials. Based on the mineral assemblage paragenetic associated with analcime, the diagenetic environment of the Jingjingzigou Formation rocks should be a freshwater–brackish water environment (Ji, 2016). The glauconite clastic mineral was commonly found in the sandstone reservoir and appeared emerald green under the microscope (Figure 8C). Glauconite of nonmarine origin is generally considered to be formed under weakly alkaline conditions, with a pH value of 7–8, and its formation is closely related to biological and biochemical processes. Based on the previous understanding of the sedimentary environment of the area, a comprehensive analysis revealed that the glauconite in the Jingjingzigou Formation could be the product of the gradual salinization of the lacustrine, weakly alkaline water medium and the weakening of hydrodynamic conditions during the epidiagenetic stage (Xing et al., 1982; Li et al., 1996).

Moreover, the results of fluid inclusions indicate that analcime were formed in relatively low temperature and brackish water environments (Figure 7D). In terms of results chemical composition, the analcime was slightly rich in aluminium and poor in sodium. The Si/Al ratios fell within the typical range for analcime of lacustrine origin (Si/Al ratio between 1.95 and 2.80). This indicates that the analcime was formed through the interaction of moderate volcanic substances and alkaline water, with the containing low level of SiO_2 activity (Han et al., 2007; Karakaya et al., 2013; Zhu et al., 2020).

Based on the 1) analcime mainly filling the intergranular pores, 2) resulting in a significant weakening of the sandstone compaction (Figure 4C), and 3) the relatively low temperature and salinity of fluid inclusions, it can be concluded that analcime is a product of the early diagenetic stage. During this stage, the volcanic substances present in large amounts in the rocks were hydrolysed by the formation water, releasing large amounts of sodium, aluminium, and silicon ions. This process increased the pH and salinity of the solution, leading to the formation of analcime under appropriate temperature and pressure conditions. Additionally, the precipitation of calcium ions facilitated the subsequent precipitation of calcite (Zhu et al., 2011). In addition to analcime, there were euhedral columnar minerals that were entirely replaced by calcite. Some intervals showed a symbiosis relationship between analcime and intact crystals filling the intergranular pores (Figure 8B). It is possible that a zeolite mineral formed without the influence of obvious acidic fluids during diagenetic evolution and was completely replaced by calcite. Under the scanning electron microscope, laumontite was observed to be paragenetic with analcime, though it was not completely replaced in certain intervals (Figure 5D).

TABLE 2 Electron microprobe analysis of analcime, albite and sphene (unit: wt%).

Sample ID	Wells	Depth (m)	Elemental composition (wt%)											Si/Al	Mineral
			Na_2O	MgO	K_2O	CaO	TiO_2	SiO_2	Al_2O_3	FeO	MnO	Cr_2O_3	Total		
101-A	S101	3043.58	13.110	0.028	0.000	0.376	0.000	56.049	24.005	0.001	0.010	0.003	93.582	1.98	Analcime
101-A	S101	3043.58	11.470	0.000	0.010	0.292	0.000	58.278	23.790	0.034	0.001	0.000	93.875	2.08	Analcime
101-A	S101	3043.58	11.276	0.004	0.018	0.212	0.017	57.916	23.496	0.050	0.000	0.010	92.999	2.09	Analcime
101-A	S101	3043.58	10.580	0.000	0.015	0.207	0.034	59.413	23.276	0.008	0.009	0.008	93.550	2.17	Analcime
101-L	S101	3261.40	12.481	0.000	0.031	0.012	0.000	56.371	23.106	0.073	0.000	0.000	92.074	2.07	Analcime
101-L	S101	3261.40	10.679	0.000	0.023	0.023	0.029	58.142	24.296	0.114	0.018	0.012	93.336	2.03	Analcime
101-L	S101	3261.40	11.185	0.000	0.026	0.005	0.000	56.831	23.359	0.144	0.014	0.000	91.564	2.06	Analcime
101-L	S101	3261.40	10.463	0.001	0.030	0.000	0.000	58.763	22.842	0.077	0.008	0.000	92.184	2.18	Analcime
101-L	S101	3261.40	10.623	0.012	0.000	0.034	0.014	58.533	23.248	0.155	0.002	0.000	92.621	2.14	Analcime
101-L	S101	3261.40	9.759	0.019	0.026	0.003	0.000	59.390	23.152	0.123	0.010	0.000	92.482	2.18	Analcime
101-L	S101	3261.40	9.582	0.013	0.004	0.031	0.000	59.086	23.511	0.118	0.010	0.000	92.355	2.13	Analcime
1-3H-A	S104-1–3H	3692.00	11.659	0.000	0.044	0.076	0.011	58.382	21.826	0.039	0.000	0.019	92.056	2.27	Analcime
1-3H-A	S104-1–3H	3692.00	11.050	0.019	0.071	0.058	0.016	59.198	21.125	0.010	0.000	0.003	91.550	2.38	Analcime
1-3H-A	S104-1–3H	3692.00	11.750	0.008	0.067	0.048	0.013	57.884	21.698	0.020	0.011	0.006	91.505	2.26	Analcime
101-L	S101	3261.40	11.823	0.012	0.037	0.039	0.000	69.023	19.902	0.033	0.000	0.014	100.883	99.61	Albite
101-L	S101	3261.40	11.663	0.025	0.149	0.041	0.005	68.536	20.188	0.155	0.006	0.000	100.768	98.98	Albite
101-L	S101	3261.40	11.946	0.014	0.054	0.049	0.036	68.939	19.984	0.094	0.000	0.023	101.139	99.48	Albite
6-F	S6	3421.50	11.875	0.008	0.080	0.066	0.004	69.873	19.595	0.006	0.000	0.000	101.507	99.26	Albite
6-F	S6	3421.50	11.678	0.025	0.037	0.128	0.009	69.648	19.729	0.009	0.003	0.004	101.270	99.19	Albite
6-F	S6	3421.50	0.030	0.021	0.001	28.656	32.294	31.077	5.090	0.552	0.005	0.029	97.755	—	Sphene
6-F	S6	3421.50	0.058	0.019	0.011	28.835	31.418	31.024	5.292	0.540	0.000	0.000	97.197	—	Sphene

10.3389/feart.2024.1416594

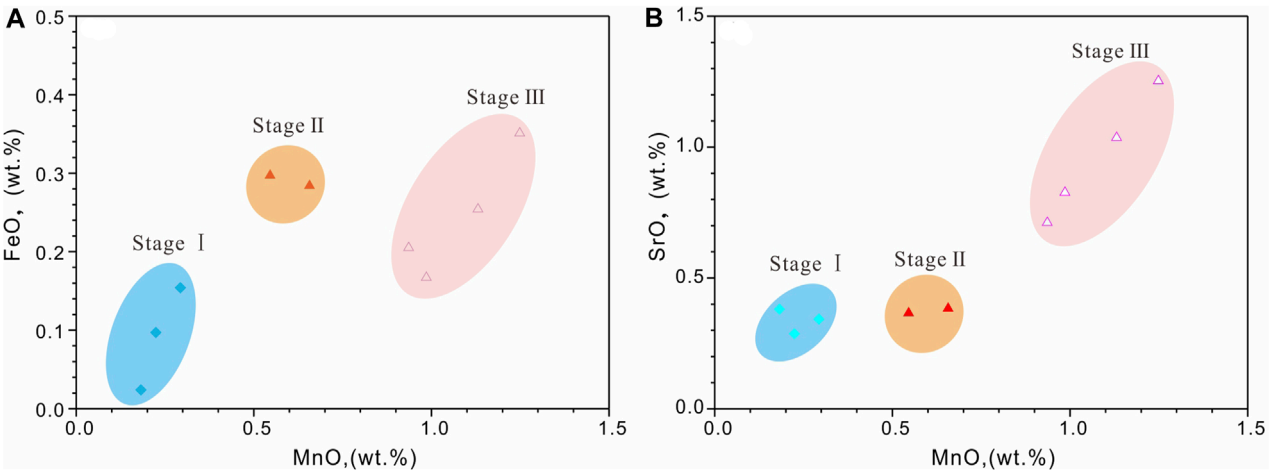

FIGURE 6
Relationship of between MnO-FeO content **(A)** and MnO-SrO content **(B)** the stage division of calcite.

TABLE 3 Analytical data: Fluid inclusion homogenization temperatures (Th), ice temperatures (Tm) and salinity of the Permian Jingjingzigou Formation.

Well name	Formation	Depth (m)	Sample ID	Lithology	FI type	Th aq (°C)	Tm aq (°C)	Sal (wt%)
S101	P_2jj	3043.58	S101FI-A	Anl	Pr	85.1	−0.8	1.40
S101	P_2jj	3255.07	S101FI-C	Anl	Pr	81.8	−1.3	2.24
S101	P_2jj	3261.40	S101FI-L	Anl	Pr	80.2	−1.2	2.07
S101	P_2jj	3261.40	S101FI-L	Anl	Pr	82.3	−1.2	2.07
S101	P_2jj	3261.40	S101FI-L	Anl	Pr	83.0	−1.0	1.74
S101	P_2jj	3261.40	S101FI-L	Anl	Pr	81.9	−1.1	1.91
S101	P_2jj	3261.40	S101FI-L	Anl	Pr	80.5	−1.3	2.07
S101	P_2jj	3261.40	S101FI-L	Anl	Pr	78.5	−1.0	1.74
S101	P_2jj	3262.52	S101FI-N	Anl	Pr	82.3	−0.9	1.57
S101	P_2jj	3262.52	S101FI-N	Anl	Pr	83.4	−0.8	1.40

Th aq, homogenization temperatures of aqueous inclusions; Tm aq, ice melting temperatures of the aqueous inclusions; Sal (wt%), salinity computed from NaCl-H_2O, system; Pr, primary; Anl, analcime.

During the diagenesis process, albite was mainly formed in the following manners (Yang et al., 2003; Zhu et al., 2011): 1) Albitization related to replacement. As the burial depth increased, the temperature and pressure also increased, leading to ion exchange between pore water and clastic substances. 2) Authigenic albite associated with the dissolution of feldspar grains. In the early stage of diagenesis, sodium ions released by the dissolution of feldspar clastic grains reached saturation levels, causing them to grow and adhere to the feldspar clastic grains, forming secondary enlarged edges. Later, as diagenesis intensified, the feldspar clastic grains further dissolved, resulting in the formation of albite. 3) During the alteration process of zeolite, under the influence of chemical factors in the formation water, the SiO_2 activity significantly increased, leading to the replacement of analcime by albite under specific conditions of temperature, pressure, and burial depth conditions (Fathy et al., 2023). In the reservoirs of the Jingjingzigou Formation in the study area, albite was produced as metasomatized plagioclase clastic grains, secondary enlargement edges, or analcime-filled dissolution pores, and authigenic albite was linked to feldspar particle dissolution. The albite filling the intergranular pores in Well S101 and other wells was paragenetic with analcime, originating mainly from the diagenetic transformation of analcime. The albite in Well S6 and other wells, not paragenetic with analcime but authigenic sphene, could be influenced by various factors. Sphene is a diagenetic product of the middle and late diagenetic stages in a freshwater to brackish water environment (Ji, 2016), and its occurrence significantly predates the precipitation of ferrocalcite in this well, indicating an earlier diagenetic period product. Earlier studies revealed that SiO_2-rich hydrothermal fluid activity during the Late Jurassic–Early Cretaceous (middle Yanshanian)

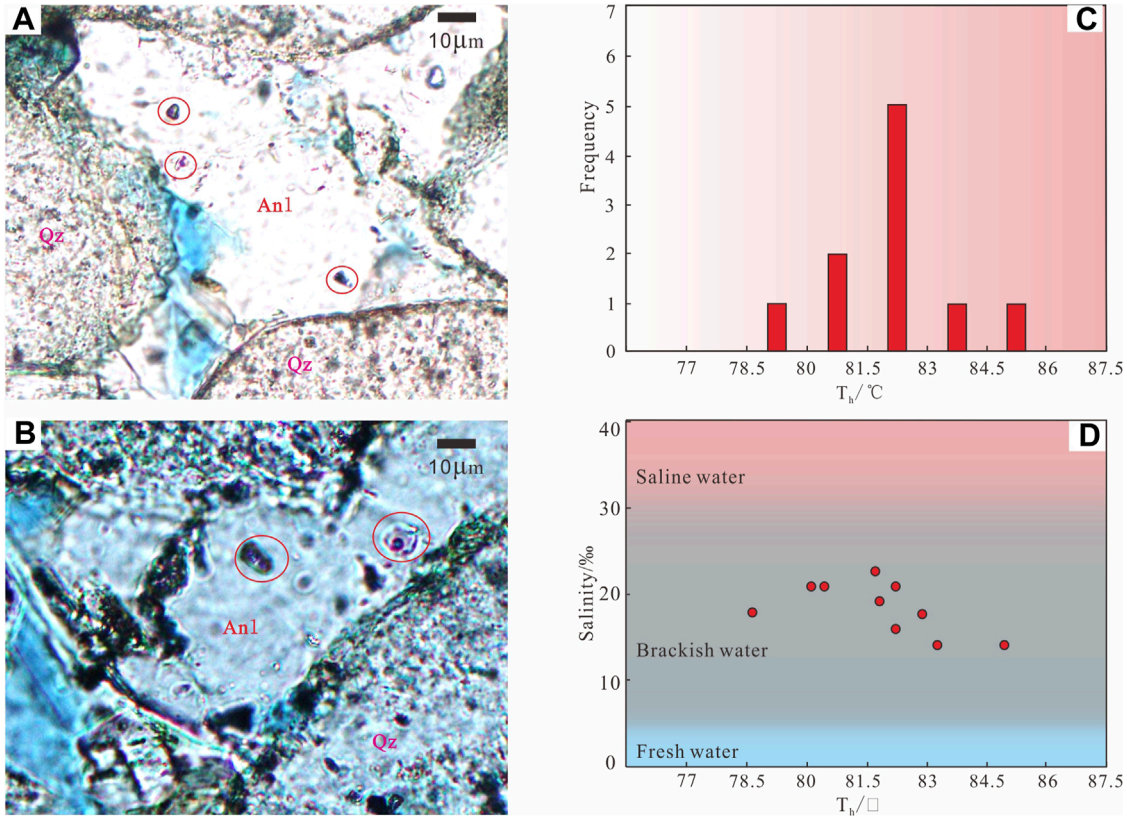

FIGURE 7
Characteristics of fluid inclusion in analcime of the Permian Jingjingzigou Formation in the Jinan Sag. **(A)** and **(B)** are photographs of fluid-inclusion in analcime cement. **(C)** Histogram of fluid-inclusion homogenization temperature (Th). **(D)** Crossplots of fluid inclusion homogenization temperature against salinity for analcime cement. The red circle are typical fluid inclusions. Anl: analcime; Qz: quartz.

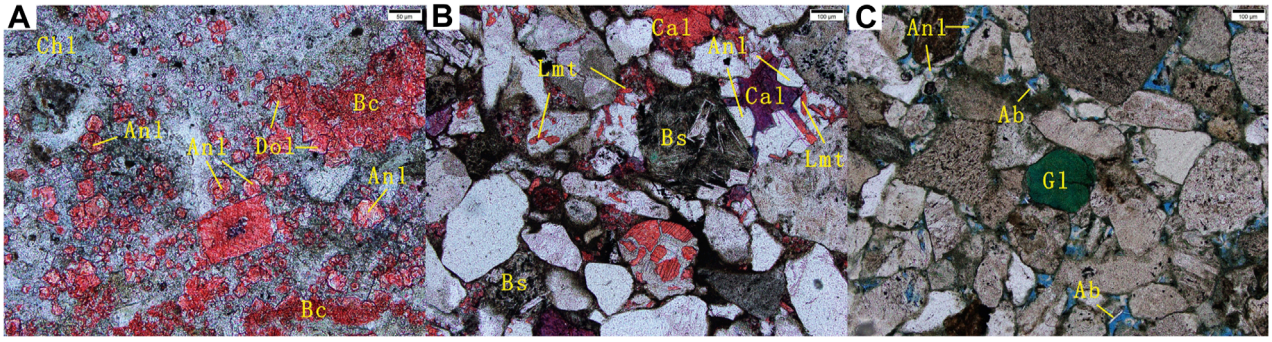

FIGURE 8
Other minerals associated with analcime formation in the study area. **(A)** Granular analcime was replaced by calcite and dolomite along the bioclastic edge developed in the tuffite (Well S4, 3221.33 m). **(B)** The intergranular filling of analcime did not undergo significant corrosion. Columnar mineral crystals (laumontite) were replaced by calcite, and the residual pores were filled with ferroan calcite (Well S104, 3435.90 m). **(C)** Emerald green glauconite spherules were found in lithic sandstone, and crescent-shaped analcime and lath-shaped analcimes were dissolved in the intergranular pores filled with albite (Well S101, 3261.40 m) (red in ab is alizarin red staining, blue in c is epoxidized resin). Chl: chlorite; Anl: analcime; BD: basalt debris; Dol: dolomite; Ab: albite; Cal: calcite; Fc: ferrocalcite; Lmt: laumontite; Glt: Glauconite.

induced the precipitation of albite and hydrothermal sphene in the secondary pores of the carboniferous pyroclastic rocks in the Kelamei area in the hinterland of the basin, leading to improved reservoir performance. The sphene from neighboring areas of the Jinan area and the Kelamei area exhibited similar composition characteristics (Table 2) and was found concurrently with albite

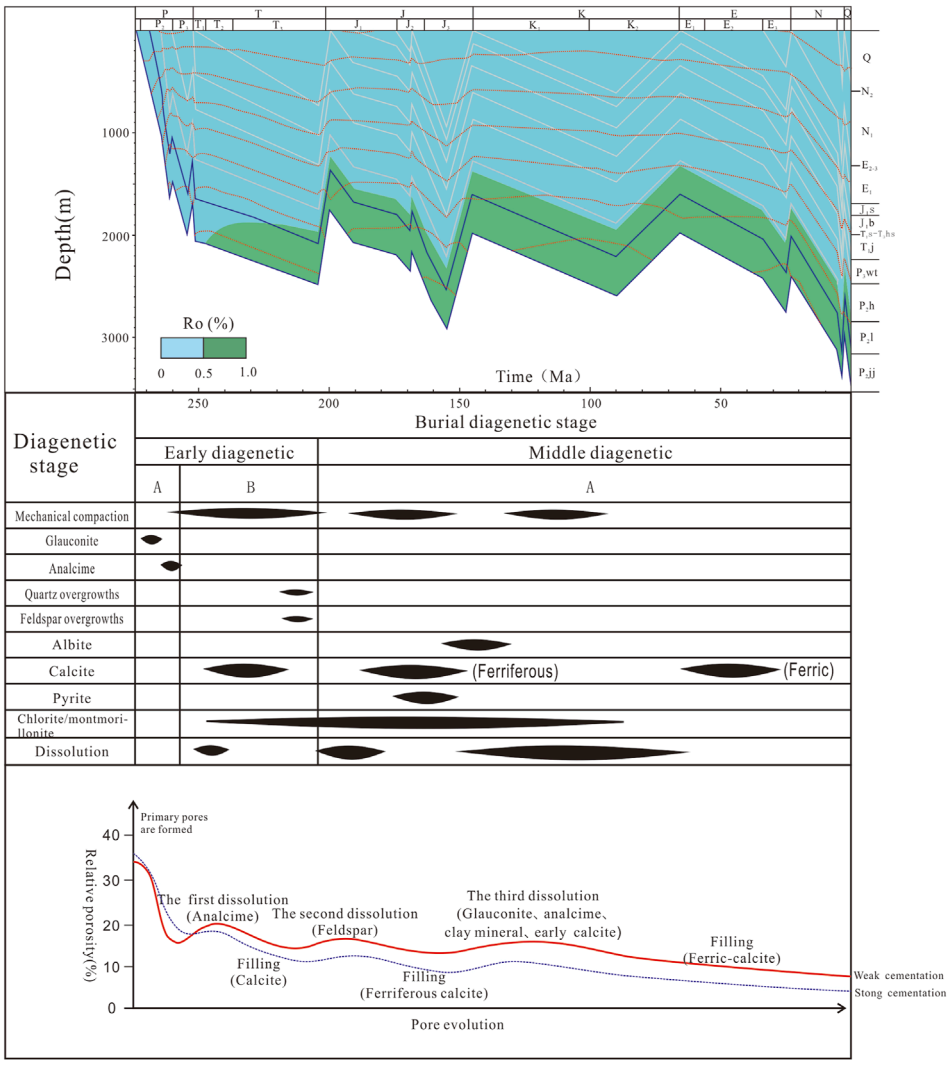

FIGURE 9
Burial diagenesis and pore evolution diagram of the Jingjingzigou Formation in the well S101.

in intergranular pores, potentially affected by higher temperatures, SiO_2-rich thermal fluid activity, and hydrocarbon charging during this period (Liu et al., 2022a, 2022b).

5.2 Burial diagenetic evolution sequence related to analcime

The burial thermal evolution history restoration results indicated that during the middle Permian, despite the overall subsidence of the Zhundong area, the southern Jinan area experienced minimal subsidence, preventing the hydrocarbon source rocks from reaching the hydrocarbon generating threshold (Figure 9). In the Early and Middle Jurassic, following a significant tectonic uplift in the Indosinian period at the end of the Late Triassic, the strata in the southern Jilin area continued to subside, leading the hydrocarbon source rocks to advance to the low mature–mature stage. Despite the subsequent uplift during the Yanshanian and Himalayan periods, resulting in substantial uplift of the hanging wall of the Fukang fault zone, the hydrocarbon source rocks remained stagnant during hydrocarbon formation. Conversely, the Jinan Sag was within the buried zone of the footwall of the fault zone, allowing the hydrocarbon source rocks to stay deeply buried and evolve to the mature stage during the Cenozoic. The Jingjingzigou Formation underwent three periods of oil accumulation during the middle and late Permian, middle and late Jurassic, and the late Neogene. The first accumulation phase occurred due to the lateral long-distance migration of mature crude oil from the neighboring Bogda rift (which includes the hanging wall of the Fukang fault zone). Towards the end of reservoir formation, crude oil generated by the hydrocarbon source rocks in the Jinan Sag collected towards the eastern and northern high points (Li et al., 2023).

Based on the characteristics of sandstone pore development and the relationship between mineral paragenesis assemblage, the Jingjingzigou Formation in the study area went through three stages of calcite filling after early chlorite and analcime

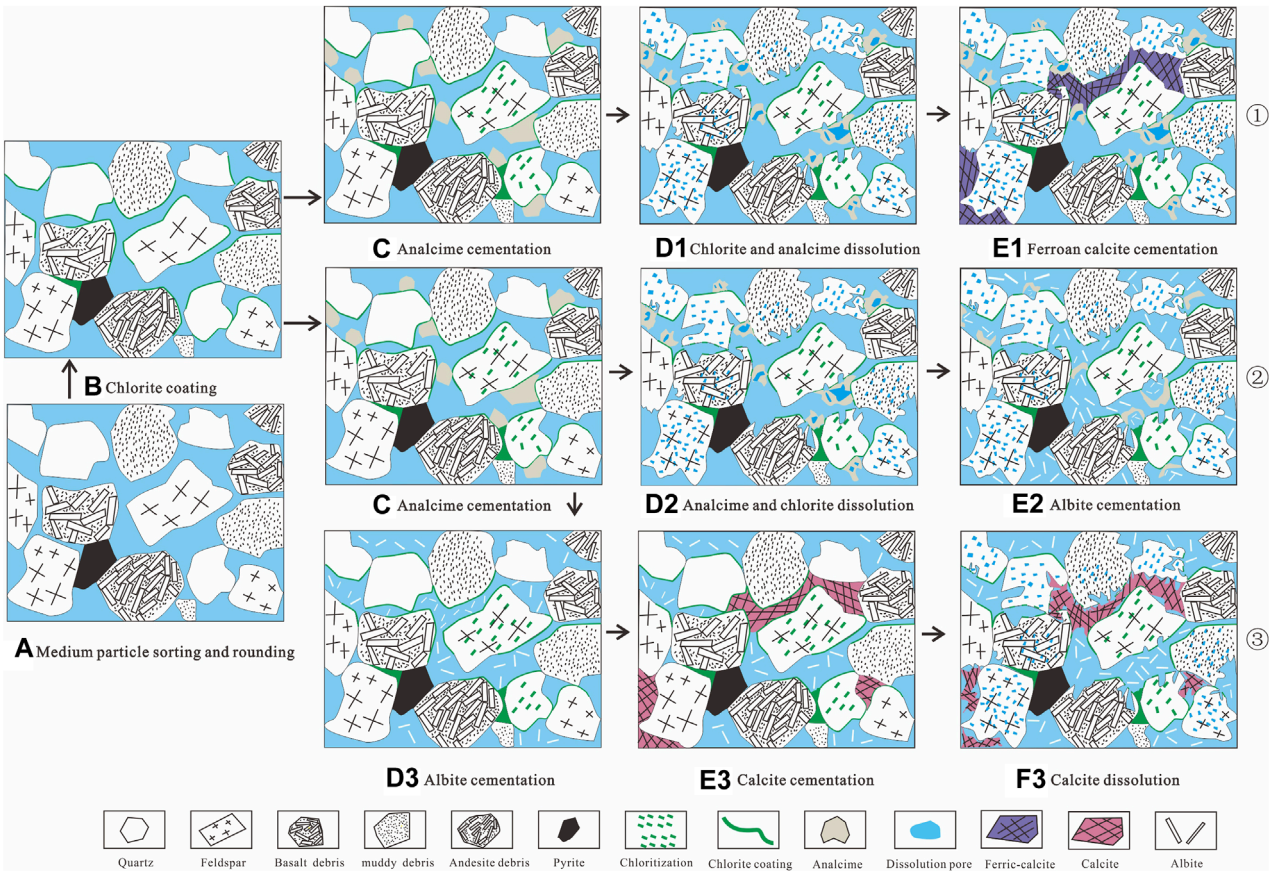

FIGURE 10
Diagram of the high-quality reservoir formation related with analcime in the study area. Three typical diagenetic evolution processes (①②③) are proposed.

mineral cementation. Additionally, it underwent at least three stages of dissolution of diagenetic minerals to varying degrees: 1) dissolution of chlorite and analcime; 2) initial dissolution of calcite; and 3) secondary dissolution of calcite. The first stage of dissolution occurred during the immature stage of hydrocarbon source rocks and could be linked to the early phase of hydrocarbon charge through lateral long-distance migration. The third stage of dissolution was observed in sections where calcite had not developed, characterized by significant corrosion of clastic feldspar, debris, and early chlorite and analcime cement, accompanied by the precipitation of authigenic albite minerals. Based on the fabrics of sandstone, pore types, degree of clay mineral evolution, and relationship between mineral paragenesis, in addition to burial thermal evolution history and hydrocarbon charging history, the diagenetic stages of the Jingjingzigou Formation reservoirs in the study area could be classified as middle diagenesis stage A (Figure 9).

5.3 Impact of analcime related diagenesis on reservoir quality

In summary, during the epidiagenetic stage, the formation of the chlorite film partially hindered the compaction and pressure solution processes. This film also preserved some primary intergranular pores, and reduced the occurrence of secondary quartz enlargement (Surdam et al., 1989; Worden et al., 2020). In the early stage of diagenesis, the precipitation and filling of analcime disrupted the primary pore structure of the sandstone, resulting in a decrease in reservoir porosity. In the middle and late stages of diagenesis, low-silicon analcime readily dissolved in organic acids or acidic pore fluids, transforming into albite. The secondary pores formed by the dissolution or transformation of analcime significantly enhanced the physical properties. The filling of calcite, which formed slightly later than the third stage of dissolution, greatly reduced porosity. Early calcite dissolution could enhance reservoir performance to some extent, but the degree of corrosion was generally not significant, and the improvement effect on the reservoir was not significant either. As a result, the pore formation and evolution of the Jingjingzigou Formation reservoirs in the study area have been determined, as illustrated in Figure 10. The formation of high-quality reservoirs related to analcime can be attributed to three crucial diagenetic processes: 1) moderate dissolution (Figure 10①), 2) relatively intense dissolution (Figure 10②), and 3) intense dissolution (Figure 10③).

Chlorite was the earliest cement formed in the reservoir, and its cementation preserved part of the primary pore space (Figures 10A,B). Subsequently, the precipitation of analcime caused

a reduction of pore (Figure 10C). The release of mature organic acids from hydrocarbon source rocks led to partial dissolution of analcime, but some pores subsequently being filled with ferroan calcite, resulting in moderate dissolution (Figures 10D1, E1). In contrast, areas with partially intensive dissolution experienced extensive dissolution of analcime followed by burial. Under appropriate temperature and pressure conditions, authigenic albite formed, leading to relatively intense dissolution (Figure 10C, D2, E2). Furthermore, in certain wells, reservoirs were clearly influenced by deep hydrothermal fluids and organic acids associated with the second stage of hydrocarbon charging. The dissolution of analcime and precipitation of albite occurred nearly simultaneously. Moreover, the analcime was completely dissolved, and the intergranular space was primarily composed of authigenic albite. Subsequently, some pores were filled with ferroan calcite, and the pores further dissolved under the influence of acidic fluids in the later stage, resulting in intense dissolution (Figures 10D3, E3, F3).

In comparison to other petroliferous basins rich in analcime worldwide, whether unconventional shale oil/gas of fine-grained sediments (Eocene Green River Formation in North America) or tight sandstone reservoir (western and eastern China) (Wang et al., 2022), porosity is mainly proportional to analcime content. However, it is important to know that the formation of high-quality reservoir is closely related to analcime, heavily influenced by factors such as volcanism, sedimentary environment, and diagenetic stage configuration. Furthermore, the development of dissolution pores within analcime has a certain degree of zoning. It is necessary to consider the limitations of being controlled laterally by sedimentary facies and provenances, and vertically by deep-buried diagenesis.

6 Conclusion

(1) The sandstone reservoirs of the Permian Jingjingzigou Formation in the Jinan sag (Junggar Basin, northwest China) primarily consist of lithic sandstone. The dominant debris present in these reservoirs is intermediate to basic extrusive rock. Analcime, clay, albite, and calcite are commonly found in these reservoirs, exhibiting differential dissolution. They either transform into albite or are replaced by other minerals. The main types of pores observed are intragranular dissolution pores of analcime.

(2) Analcime is characterized by its high aluminium content, low sodium content, and low Si/Al ratio. It forms during the early diagenetic stage when there is a significant presence of volcanic material in the rocks. This formation occurs under the influence of alkaline formation water, along with suitable temperature and pressure conditions. During the early diagenetic stage, analcime precipitates and fills the intergranular pores, which can result in damage to the structure of the primary pore and a reduction in porosity. The middle diagenetic stage is characterized by the formation of secondary pores through the dissolution of chlorite, analcime, and certain carbonate minerals. This process enhances the reservoir properties.

(3) In sandstone reservoirs with abnormally developed secondary pores at the similar sedimentary environments, it is essential for identify whether the presence of early analcime cement. Besides, to effectively distinguish the controlled factors requires combination of the mineral paragenesis relationship and experiments, it is helpful for quantitatively assess the effects of analcime precipitation-dissolution of deep clastic reservoirs during burial stage.

Data availability statement

The original contributions presented in the study are included in the article/Supplementary Material, further inquiries can be directed to the corresponding author.

Author contributions

TL: Conceptualization, Methodology, Writing–original draft. WW: Formal Analysis, Investigation, Writing–review and editing. QM: Data curation, Software, Writing–review and editing. JK: Software, Writing–review and editing. RY: Software, Writing–review and editing. XL: Data curation, Supervision, Validation, Writing–review and editing.

Funding

The author(s) declare that financial support was received for the research, authorship, and/or publication of this article. This work was supported by the Enterprise Innovation and Development Joint Fund National Natural Science Foundation of China (U22B6002); and The Xinjiang Uygur Autonomous Region "Tianshan Talents" Scientific and Technological Innovation Leading Talents Support Project (2022TSYCLJ0070); and the Scientific Research and Technology Development Project of China National Petroleum Corporation (2023YQX10109).

Conflict of interest

Authors TL and RY were employed by the PetroChina. Author WW was employed by the Sinopec Henan Oil-field Company. Authors QM and JK were employed by the Tuha Oilfield Company, PetroChina.

The remaining author declares that the research was conducted in the absence of any commercial or financial relationships that could be construed as a potential conflict of interest.

Publisher's note

References

Campo, M. D., Papa, C. D., Jiménez-Millán, J., and Nieto, F. (2007). Clay mineral assemblages and analcime formation in a Palaeogene fluvial-lacustrine sequence (MaízGordo Formation Palaeogen) from northwestern Argentina. *Sediment. Geol.* 201 (1-2), 56–74. doi:10.1016/j.sedgeo.2007.04.007

Dutton, S. P., and Loucks, R. G. (2010). Reprint of: diagenetic controls on evolution of porosity and permeability in lower Tertiary Wilcox sandstones from shallow to ultradeep (200–6700 m) burial. Gulf of Mexico Basin, USA. *Mar. Pet. Geol.* 27 (1), 1775–1787. doi:10.1016/j.marpetgeo.2009.12.010

English, P. M. (2001). Formation of analcime and moganite at Lake Lewis, central Australia: significance of groundwater evolution in diagenesis. *Sediment. Geol.* 143 (3), 219–244. doi:10.1016/S0037-0738(01)00063-X

Fang, R., Dai, Z. Y., Chen, Z. J., Shan, J. F., Jin, K., and Zhang, Y. F. (2020). Characteristics and genesis of analcites in different occurrence states: a case study of the fourth member of Shahejie Formation in the Leijia area of the Western Liaohe Depression. *Acta mineralogica sinica*. 40 (6), 734–764. doi:10.16461/j.cnki.1000-4734.2020.40.155

Fathy, D., Abart, R., Wangreich, N., Gier, S., Ahmed, M., and Sami, M. (2023). Late campanian climatic-continental weathering assessment and its influence on source rocks deposition in southern tethys, Egypt. *Minerals* 13 (2), 160. doi:10.3390/min13020160

Fu, G. M., Dong, M. C., Zhang, Z. S., et al. (2010). Formation process and distribution of laumontite in Yanchang 3 reservoir of Fuxian exploration area in north Shaanxi province and the controls of the high-quality reservoirs. *Earth Sci. J. China Univ. Geosci.* 35 (1), 107–114. doi:10.3799/dqkx.2010.011e

Gall, Q., and Hyde, R. (2010). Analcime in lake and lake-margin sediments of the carboniferous Rocky Brook Formation, western newfoundland, Canada. *Sedimentology* 36 (5), 875–887. doi:10.1111/j.1365-3091.1989.tb01751.x

Gao, C., Meng, S., Zhang, J., Wang, J., and Sun, Y. (2023). Effects of cementation on physical properties of clastic rock-originated weathering crust reservoirs in the Kexia region, Junggar Basin, NW China. *Energy Geoscience* 4 (1), 74–82. doi:10.1016/j.engeos.2022.08.006

Guo, H., Ji, B. Q., Yang, S., Wang, R., Zhang, S. C., Li, J. S., et al. (2022). Formation of zeolite cement in Permian sandy conglomerate reservoir in the circumMahu sag, Junggar Basin and its petroleum geological significance. *Acta Pet. Sin.* 43 (03), 341–354. doi:10.7623/syxb202203002

Han, S. H., Yu, H. Z., Si, C. S., Chen, S. H., Chen, N. G., and Yu, L. (2007). Corrosion of analcite in reservoir of Junggar Basin. *Acta Pet. Sin.* (3), 51–54+62. doi:10.7623/syxb200703010

Sheppard, R. A., and Hay, R. L. (2001). Occurrence of zeolites in sedimentary rocks: an overview. *Rev. Mineral. Geochem.* 45 (1), 217–234. doi:10.2138/rmg.2001.45.6

Iijima, A. (2001). 12. Zeolites in petroleum and natural gas reservoirs. *Rev. Mineral. Geochem.*, 347–402. doi:10.1515/9781501509117-014

Ji, Y. L. (2016). *Oil and gas reservoir Geology*. China University of Petroleum Press, 64–72.

Jia, C. Z., Pang, X. Q., and Jiang, F. J. (2016). Research status and development directions of hydrocarbon resources in China. *Petroleum Sci. Bull.* 1 (01), 2–23. doi:10.3969/j.issn.2096-1693.2016.01.001

Jin, H. N., and Boles, J. R. (1993). Origin of zeolite cements in the Miocene sandstones, north tejon oil fields, California. *J. Sediment. Res.* 63 (2), 248–260. doi:10.1306/D4267AD2-2B26-11D7-8648000102C1865D

Karakaya, N., Muazzez, C. K., and Temel, A. (2013). Mineralogical and chemical properties and the origin of two types of analcime in SW Ankara, Turkey. *Clays Clay Minerals* 61 (3), 231–257. doi:10.1346/CCMN.2013.0610306

Langella, A., Cappelletti, P., and Gennaro, R. D. (2001). Zeolites in closed hydrologic systems. *Rev. Mineral. Geochem.* 45 (1), 235–260. doi:10.2138/rmg.2001.45.7

Li, J., Zhang, W. J., Xiang, B. L., He, D., Yang, S. C., Wang, J., et al. (2022). Characteristics of dissolved pores and dissolution mechanism of zeolite-rich reservoirs in the Wuerhe Formation in Mahu area, Junggar Basin. *Energy Explor. Exploitation* 40 (1), 421–441. doi:10.1177/01445987211028732

Li, J. S., Fu, L., Zhang, J. L., Chen, J., Niu, B., and Zhang, S. C. (2019). Diagenesis and secondary pore evolution of Middle and Upper Permian clastic rocks in Wu-Xia area, Junggar Basin. *Lithol. Reserv.* 31 (6), 54–66. doi:10.12108/yxyqc.20190606

Li, J. Z., Chen, X., Yang, R. Z., Lin, T., Yang, F., Ma, Q., et al. (2023). Petroleum geology and sub-source hydrocarbon accumulation of Permian reservoirs in Jinan Sag, eastern Junggar Basin, NW China. *Petroleum Explor. Dev.* 50 (3), 558–572. doi:10.1016/s1876-3804(23)60410-0

Li, Z. H., Qiu, L. W., Shi, Z., Tang, Y., Kong, Y. H., and Zhu, S. B. (2014). Diagenesis of zeolite minerals and its significance for hydrocarbon accumulation in the second member of Jiamuhe formation of Zhongguai area, Junggar Basin. *J. China Univ. Petroleum*. 38 (01), 1–7. doi:10.3969/jissn.1673-5005.2014.01.001

Liang, S. J., Luo, Q. S., Kang, J. L., Li, F. L., Ma, Q., Wang, X. C., et al. (2021). Breakthrough and significance of risk exploration in well satan 1 in jinan sag, Junggar Basin. *China Pet. Explor.* 26 (4), 72–83. doi:10.3969/j.issn.1672-7703.2021.04.00

Lin, P. X., Lin, C. M., Yao, Y., Wang, B. J., Li, L., Zhang, X., et al. (2017). Characteristics and causes of analcime distributed in dolostone of the Member 3 of Paleogene Shahejie Formation in Beitang sag, Bohai Bay Basin. *Journal of Palaeogeography* 19 (2), 241–256. doi:10.7605/gdlxb.2017.02.019

Liu, X. H., Wang, W. W., Feng, M. Y., Zhuo, Y. Q., and Yue, H. H. (2022a). Hydrothermal process and duration of carboniferous altered tuff reservoir in well dixi 14 area of kelameili gas field (Junggar Basin), NW China. *Earth Sci.* 47 (5), 1694–1710. doi:10.3799/dqkx.2021.188

Liu, X. H., Zhuo, Y. Q., Feng, M. Y., Zhang, B. J., Xia, M. L., and Wang, X. Z. (2022b). Constrains of eruption environment and hydrothermal fluid on the Permian pyroclastic reservoirs in the Sichuan Basin, SW China. *Petroleum* 8, 17–30. doi:10.1016/j.petlm.2021.03.005

Meng, Y. L., Liang, H. T., Wei, W., et al. (2013). Thermodynamic calculations of the laumontite dissolution and prediction of secondary porosity zones: a case study of horizon of Xujiaweizi fault depression. *Acta Sedimentol. Sin.* 31 (3), 509–515. doi:10.1016/j.petlm.2021.03.005

Neuhoff, P. S. (2002). Natural zeolites: occurrence, properties, applications. *Am. Mineralogist* 45 (11-12), 1737–1738.

Noh, J. H., and Boles, J. R. (1993). Origin of zeolite cements in the Miocene sandstones, North Tejon oil f-ields, California. Sediment. *Res* 63 (2), 248–260. doi:10.1306/d4267ad2-2b26-11d7.8648000102c1865d

Renaut, R. W. (1993). Zeolitic diagenesis of late Quaternary fluviolacustrine sediments and associated calcrete formation in the Lake Bogoria Basin, Kenya Rift Valley. *Sedimentology* 40 (2), 271–301. doi:10.1111/j.1365-3091.1993.tb01764.x

Schmidt, V., and McDonald, D. A. (1979). The role of secondary porosity in the course of sandstone diagenesis. *SPEM Spec. Publ.* 26, 175–207. doi:10.2110/pec.79.26.0175

Sun, Y. S., Liu, X. N., Zhang, Y. Q., Dong, W. K., Xu, Y. L., Shi, G. X., et al. (2014). Analcite cementation facies and forming mechanism of high-quality secondary clastic rock reservoirs in western China. *J. Paleogeogr.* 16 (04), 517–526. doi:10.7605/gdlxb.2014.04.042

Surdam, R. S., Crossey, L. J., Hangen, E. S., and Heasler, H. P. (1989). Organic-inorganic interaction and sandstone diagenisis. *AAPG Bull.* 73 (1), 1–23. doi:10.1306/703C9AD7-1707-11D7-8645000102C1865D

Tang, Z. H., John, P., and Fred, J. L. (1997a). Diagenesis and reservoir potential of Permian-Triassic fluvial/lacustrine sandstones in the southern Junggar basin, Northwestern China. *AAPG Bull.* 81 (11), 1843–1865. doi:10.1306/3B05C64A-172A-11D7-8645000102C1865D

Tang, Z. H., John, P., and Fred, J. L. (1997b). Diagenesis of analcime-bearing reservoir sandstones: the upper permian pingdiquan formation, Junggar Basin, Northwest China. *Sediment. Res.* 67 (3), 486–498. doi:10.1306/D42685A4-2B26-11D7-8648000102C1865D

Taylor, M. W., and Surdam, R. C. (1981). Zeolite reactions in the tuffaceous sediments at Teels marsh, Nevada. *Clay Clay Min.* 29, 341–352. doi:10.1346/ccmn.1981.0290504

Utada, M. (2001). Zeolites in burial diagenesis and low-grade metamorphic rocks. *Rev. Mineral. Geochem.* 45 (1), 277–304. doi:10.2138/rmg.2001.45.9

Varol, E. (2020). Interpretation of the origin of analcimes with mineralogical, microtextural, and geochemical investigations:a case study from Aktepe region (NE of Kalecik, Ankara,Central Anatolia, Turkey). *Arabian J. Geosciences* 13 (10), 343–410. doi:10.1007/s12517-020-05315-9

Wang, J. R., Liang, C., Cao, Y. C., and Tian, Y. (2022). Occurrence, genesis, and significance of analcime in fine-grained sedimentary rocks. *Geofluids* 2022 (2), 1–17. doi:10.1155/2022/3633047

Weibel, R., Olivarius, M., Jakobsen, F. C., Whitehouse, M., Larsen, M., Midtgard, H., et al. (2019). Thermogenetic degradation of early zeolite cement: an important process for generating anomalously high porosity and permeability in deeply buried sandstone reservoirs? *Mar. Petroleum Geol.* 103, 620–645. doi:10.1016/j.marpetgeo.2019.02.006

Worden, R. H., Utley, J. E., Butcher, A. R., Griffiths, L. J., Wooldridge, L. J., and Lawan, A. Y. (2020). Improved imaging and analysis of chlorite in reservoirs and modern day analogues: new insights for reservoir quality and provenance. *Geol. Soc. Lond. Spec. Publ.* 484 (1), 189–204. doi:10.1144/SP484.10

Wu, J. J., You, L. P., and Yang, H. S. (2013). Structural evolution and hydrocarbon accumulation of Fukang fault zone in Junggar Basin. *Xinjiang Pet. Geol.* 34 (1), 36–40. doi:10.11743/ogg20180506

Xing, S. Q., Xiao, Z. S., and Zhang, S. G. (1982). Mineralogical characteristic of glauconite and conditions of its formation in the Taikang inlet, Songliao Basin. *Acta Mineral. Sin.* (01), 52–58+85.

Yang, G. H., Zhuo, S. G., Niu, B., and E, J. J. (2003). Albitization of detrital feldspar in cretaceous sandstones from the songliao basin. *Geol. Rev.* 49 (03), 155–161+228. doi:10.16509/j.georeview.2003.02.007

Yuan, G. H., Cao, Y. C., Gluyas, J., Li, X., Xi, K., Wang, Y., et al. (2015). Feldspar dissolution, authigenic clays, and quartz cements in open and closed

sandstone geochemical systems during diagenesis: typical examples from two sags in Bohai Bay Basin, East China. *AAPG Bull.* 99 (11), 2121–2154. doi:10.1306/07101514004

Yuan, Z., Li, W. H., Yuan, H. L., and Guo, Y. Q. (2020). Pore evolution characteristic of sandstone reservoir with laumontite cement and its influence on reservoir properties: chang10_1, reservoir of Yanchang Formation in Southeast of Ordos Basin. *Chin. J. Geol.* 55 (3), 767–781. doi:10.12017/dzkx.2020.047

Zhang, P. H. (1985). Precipitation of zeolite and pore evaluation of coarse clastic rock reservoir in permian from karamay. *Xinjiang Pet. Geol.* (2), 30–47.

Zhang, Y. Q., and Zhang, N. F. (2006). Oil/gas enrichment of large superimposed basin in Junggar Basin. *China Pet. Explor.* (1), 59–6478.

Zheng, M., Li, J. Z., Wu, X. Z., Wang, S. J., Guo, Q. L., Chen, X. M., et al. (2019). Potential of oil and natural gas resources of main hydrocarbon bearing basins and Key exploration fields in China. *Earth Sci.* 44 (3), 833–847. doi:10.3799/dqkx.2019.957

Zhu, S. F., Cui, H., Jia, Y., Zhu, X. M., Tong, H., and Ma, L. C. (2020). Occurrence, composition, and origin of analcime in sedimentary rocks of non-marine petroliferous basins in China. *Mar. Petroleum Geol.* 113, 104164–104216. doi:10.1016/j.marpetgeo.2019.104164

Zhu, S. F., Zhu, X. M., Wang, X. L., and Liu, Z. Y. (2011). Zeolite diagenesis and its control on petroleum reservoir quality of Permian in northwestern margin of Junggar Basin, China. *China Sci. China Earth Sci.* 41 (11), 1602–1612. doi:10.1007/s11430-011-4314-y